Electronic Supplementary Material (ESI) for Journal of Materials Chemistry A.


# $CO_2$ electroreduction activity and dynamic structural evolution of *in situ* reduced Nickel-Indium mixed oxides

## Electronic supplementary information

*Laura C. Pardo Pérez,*[a] Zora Chalkley,[a,b] Robert Wendt,[c] Ibbi Y. Ahmet,[c] Markus Wollgarten[c] and Matthew T. Mayer*[a]*

[a] Young Investigator Group Electrochemical Conversion of $CO_2$, Helmholtz-Zentrum Berlin für Materialien und Energie GmbH, Hahn-Meitner-Platz 1, 14109 Berlin, Germany

[b] Institut für Chemie & Biochemie, Freie Universität Berlin, Berlin 14195, Germany

[c] Institute for Solar Fuels, Helmholtz-Zentrum Berlin für Materialien und Energie GmbH, Hahn-Meitner-Platz 1, 14109 Berlin, Germany

*Corresponding authors: Laura C. Pardo Pérez (lcpardop@gmail.com) and Matthew T. Mayer (m.mayer@helmholtz-berlin.de)

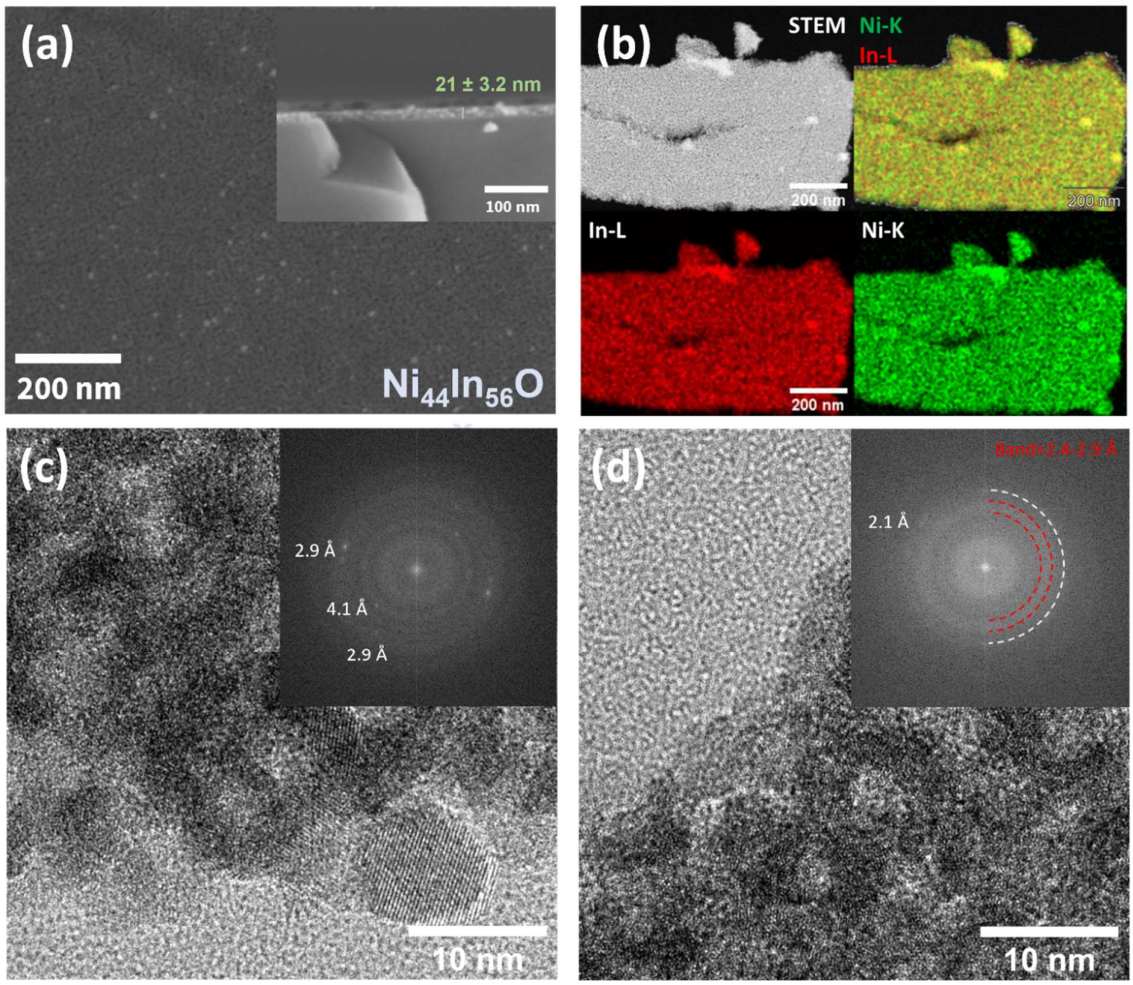


**Figure S1. Structural characterization of as synthesized $Ni_{40}In_{60}Ox$ thin film. (a) SEM micrograph. (b) STEM-EDS mapping. (c-d) HRTEM images displaying small crystallites (resolution: 0.0194 pix/nm), FFT analysis of HRTEM images are presented as inset. The Ni fraction referred total metal (Ni+In) as determined by ICP is displayed as a text inset on the SEM micrograph.**

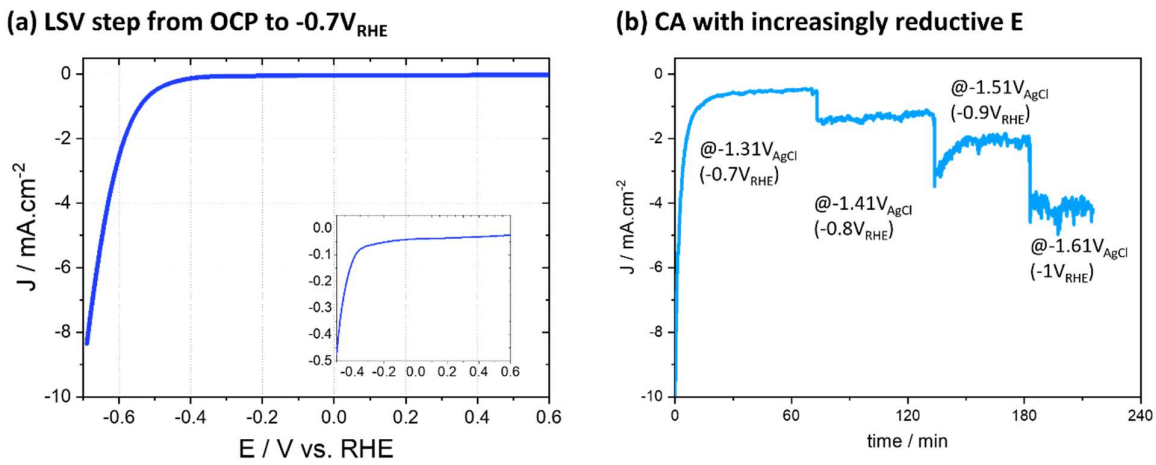


**Figure S2. Representative data of typical $CO_2$ER electrochemical test for $Ni_{50}In_{50}Ox$. (a) LSV from the measured open circuit potential (OCP) to -0.7 V vs RHE at 10 mV $s^{-1}$, followed by (b) sequence of potentiostatic electrolysis at increasingly reductive potential ranging from -0.7 V to -1.0 V at 0.1 V intervals holding each potential for 45-60 min.**

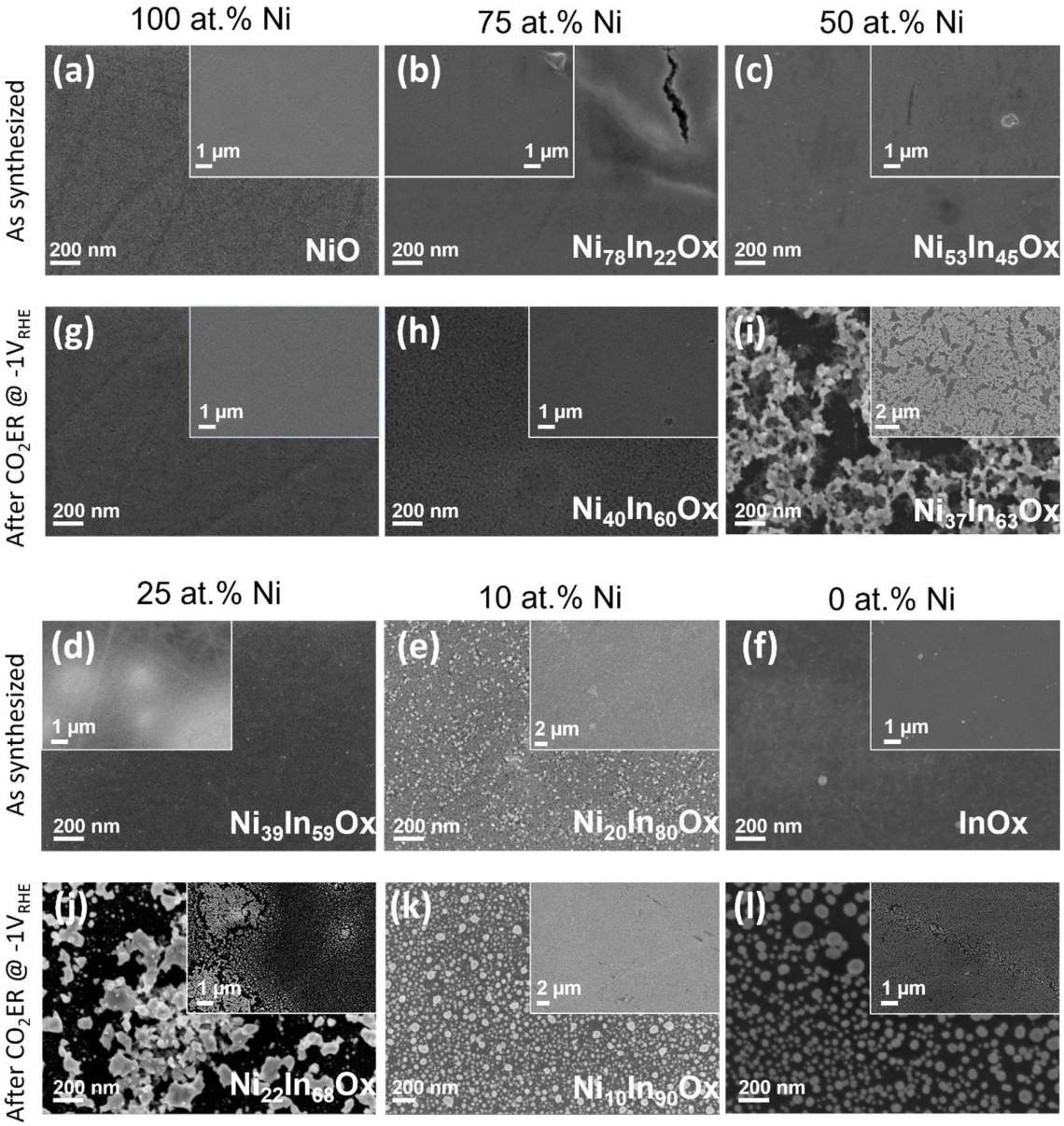


**Figure S3. SEM investigation of $Ni_AIn_BOx$ thin films morphology with nominal composition NiO, $Ni_{75}In_{25}Ox$, $Ni_{50}In_{50}Ox$, $Ni_{75}In_{25}Ox$, $Ni_{10}In_{90}Ox$ and $In_2O_3$, as synthesized (a-f) and after $CO_2$ER electrolysis test at-1.0 V (g-l). Low magnification (10kx) image is presented as inset for evaluation of homogeneity. Experimental composition found by EDS is presented as text inset on the SEM image for each sample.**

## Summary of composition analysis of Ni-In mixed oxides by EDS and ICP-OES

### Table S1. Composition analysis of $Ni_AIn_BOx$ EDS (SEM) and ICP-OES.

| $Ni_AIn_BOx$ | Nominal Ni fraction | As synthesized | | | | Ni fraction after $CO_2ER$ at - 1 V |
|---|---|---|---|---|---|---|
| | | Ni fraction | | Catalyst loading [a)] | | |
| | | SEM-EDS | ICP | µg $cm^2$ | µmol $cm^{-2}$ | SEM-EDS |
| **NiO** | 1.0 | 1.0 | 1.0 | 5.8 | 0.099 | 1.00 |
| **$Ni_{75}In_{25}O_X$** | 0.75 | 0.82 | 0.78 | 6.9 | 0.096 | 0.73 |
| **$Ni_{50}In_{50}O_X$** | 0.50 | 0.62 | 0.53 | 7.6 | 0.089 | 0.37 |
| **$Ni_{40}In_{60}O_X$** | 0.40 | 0.48 | 0.44 | 8.1 | 0.089 | 0.36 |
| **$Ni_{25}In_{75}O_X$** | 0.25 | 0.39 | 0.31 | 8.2 | 0.084 | 0.22 |
| **$Ni_{10}In_{90}O_X$** | 0.10 | 0.20 | 0.14 | 8.6 | 0.079 | <0.10 |
| **$In_2O_3$** | 0.0 | 0.0 | 0.0 | 12.6 | 0.109 | 0 |
| **$Ni_2In_3$ alloy** | 0.4 | 0.42 | 0.4 | 6.9 | 0.073 | 0.4 |

[a)] Catalyst loading in total µg or µmol of M = Ni + In per $cm^{-2}$

## Summary of surface and bulk composition analysis of $Ni_{40}In_{60}Ox$ after diverse electrochemical $CO_2ER$ experiments.

### Table S2. Composition analysis of $Ni_{40}In_{60}Ox$ by XPS, ICP-OES and EDS (SEM and TEM)

| | | XPS | | ICP-OES | | SEM-EDS | | TEM-EDS | |
|---|---|---|---|---|---|---|---|---|---|
| | | Ni fraction | Std. dev [a)] | Ni fraction | Std. dev [a)] | Ni fraction | Std. dev [b)] | Ni fraction | Std. dev [c)] |
| **$Ni_{40}In_{60}Ox$** | **As synthesized.** | 0.27 | 0.02 | 0.44 | 0.02 | 0.48 | 0.01 | 0.44 | 0.00 |
| | **-0.8 V_1h** | 0.20 | 0.02 | 0.38 | 0.02 | 0.44 | 0.04 | 0.43 | 0.00 |
| | **-0.8 V_10h** | 0.20 | 0.02 | 0.33 | 0.01 | 0.35 | 0.02 | 0.26 | 0.02 |
| | **-1 V_1h** | 0.33 | 0.02 | 0.36 | 0.01 | 0.34 | 0.02 | 0.21 | 0.03 |
| **$Ni_2In_3$ alloy** | **As synthesized.** | | | 0.40 | 0.02 | 0.42 | 0.06 | | |
| | **-1 V_1h** | | | 0.35 | 0.02 | 0.40 | 0.02 | | |

[a)] Standard deviation of quantification results measured on two or three replicate samples.

[b)] Standard deviation of quantification results measured on three different spots on at least two replicate samples.

[c)] Standard deviation of quantification results measured on two different spots of one sample.

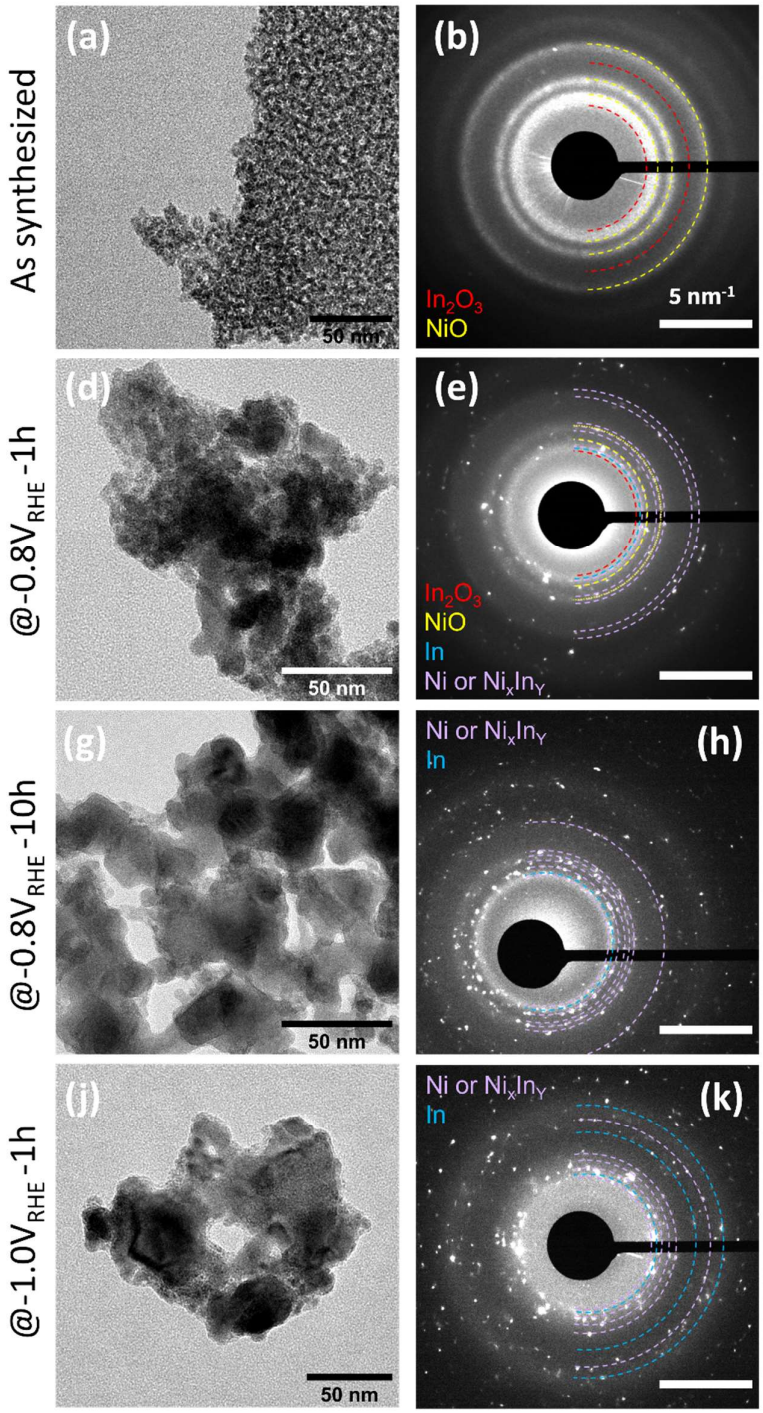


| SAED of $Ni_{40}In_{60}O_X$ As synthesized | | |
|---|---|---|
| d (Å) | Assignment | |
| 2.91 | $In_2O_3$ | |
| 2.51 | NiO | $In_2O_3$ |
| 2.14 | NiO | |
| 1.77 | $In_2O_3$ | |
| 1.52 | $In_2O_3$ | NiO |

| SAED after $CO_2$ER at -0.8V _1h | | | |
|---|---|---|---|
| d (Å) | Assignment | | |
| 2.87 | $Ni_3In_7$ | $In_2O_3$ | |
| 2.75 | In | | |
| 2.57 | $Ni_3In_7$ | | |
| 2.51 | $Ni_3In_7$ | NiO | $In_2O_3$ |
| 2.21 | Ni, $Ni_XIn_Y$ | NiO | |
| 2.11 | Ni, $Ni_XIn_Y$ | | |
| 2.05 | Ni, $Ni_XIn_Y$ | | |
| 1.58 | $Ni_3In_7$ | NiO | $In_2O_3$ |
| 1.49 | $Ni_3In$ | | |

| SAED after $CO_2$ER at -0.8V _10h | | | |
|---|---|---|---|
| d (Å) | Assignment | | |
| 2.88 | $Ni_3In_7$ | $In_2O_3$ | |
| 2.72 | In | | |
| 2.51 | $Ni_3In_7$ | NiO | $In_2O_3$ |
| 2.36 | Ni, $Ni_XIn_Y$ | NiO | |
| 2.23 | Ni, $Ni_XIn_Y$ | | |
| 2.05 | Ni, $Ni_XIn_Y$ | | |
| 1.8 | Ni, $Ni_XIn_Y$ | | $In_2O_3$ |
| 2.05 | Ni, $Ni_XIn_Y$ | | |
| 1.57 | $Ni_3In_7$ | NiO | $In_2O_3$ |
| 1.52 | $Ni_3In$ | | |

| SAED after $CO_2$ER at -1V _1h | | | |
|---|---|---|---|
| d (Å) | Assignment | | |
| 2.83 | $Ni_3In_7$ | $In_2O_3$ | |
| 2.75 | In | | |
| 2.53 | $Ni_3In_7$ | NiO | $In_2O_3$ |
| 2.3 | Ni, $Ni_XIn_Y$ | NiO | |
| 2.21 | Ni, $Ni_XIn_Y$ | | |
| 2.06 | Ni, $Ni_XIn_Y$ | | |
| 1.7 | In | | |
| 1.56 | $Ni_3In_7$ | NiO | $In_2O_3$ |
| 1.49 | $Ni_3In$ | | |
| 1.37 | In | | |

**Figure S4.TEM-SAED analysis of $Ni_{40}In_{60}Ox$ thin film at different stages of reduction during $CO_2$ER operation. From left to right TEM micrograph, associated SAED image and assignment are presented for $Ni_{40}In_{60}Ox$ thin film (a, b, c) in as synthesized condition, and after $CO_2$ER electrolysis in 0.1 M $KHCO_3$ at (d,e,f) -0.8 V for 1h; (g,h,i) -0.8 V for 10 h and (j,k,l) -1.0 V for 1h. The instrumental error of <1% for SAED measurements was determined using an Au reference.**

**Table S3. Analysis of SAED images of $Ni_{40}In_{60}Ox$ and correlation of d-spacing with possible phases.**

| d spacings for possible phases (Å) | | | | | | | | | d spacing observed in SAED for $Ni_{40}In_{60}Ox$ (Å) | | | |
|---|---|---|---|---|---|---|---|---|---|---|---|---|
| **In** | **$In_2O_3$** | **NiO** | **Ni PDF** | **Ni (COD)** | **NiIn** | **$Ni_3In$** | **$Ni_2In_3$** | **$Ni_3In_7$** | **As synth.** | **At -0.8 V 1 h** | **At - 0.8 V 10 h** | **At - 1 V 1 h** |
| | 4.13 | | | | 3.94 | | | | | | | |
| | 2.92 | | | | 2.92 | 2.97 | 3.09 | 2.91 | 2.91 | 2.87 | 2.88 | 2.83 |
| 2.72 | | | | | | | | | | 2.75 | 2.72 | 2.75 |
| | | | | | | | | 2.65 | | 2.57 | | |
| 2.48 | 2.53 | 2.55 | | | | | | 2.46 | 2.51 | 2.51 | 2.51 | 2.53 |
| 2.30 | | 2.21 | | 2.27 | 2.27 | | 2.20 | | | 2.21 | 2.36<br>2.23 | 2.30<br>2.21 |
| | | | | 2.16 | 2.17 | 2.10 | 2.17 | 2.17 | 2.14 | 2.11 | | |
| | | | 2.04 | 2.01 | 2.01 | | | 2.05 | | 2.05 | 2.05 | 2.06 |
| | 1.79 | | 1.77 | | 1.79 | | | | 1.77 | | 1.80 | |
| 1.69 | | | | | | | | 1.62 | | 1.58 | 1.57 | 1.70 |
| | 1.53 | 1.56 | | 1.57 | 1.57 | 1.48 | 1.54 | 1.58 | 1.52 | 1.49 | 1.52 | 1.49<br>1.56 |
| 1.40 | | 1.33 | | | | | | | | | | 1.37 |

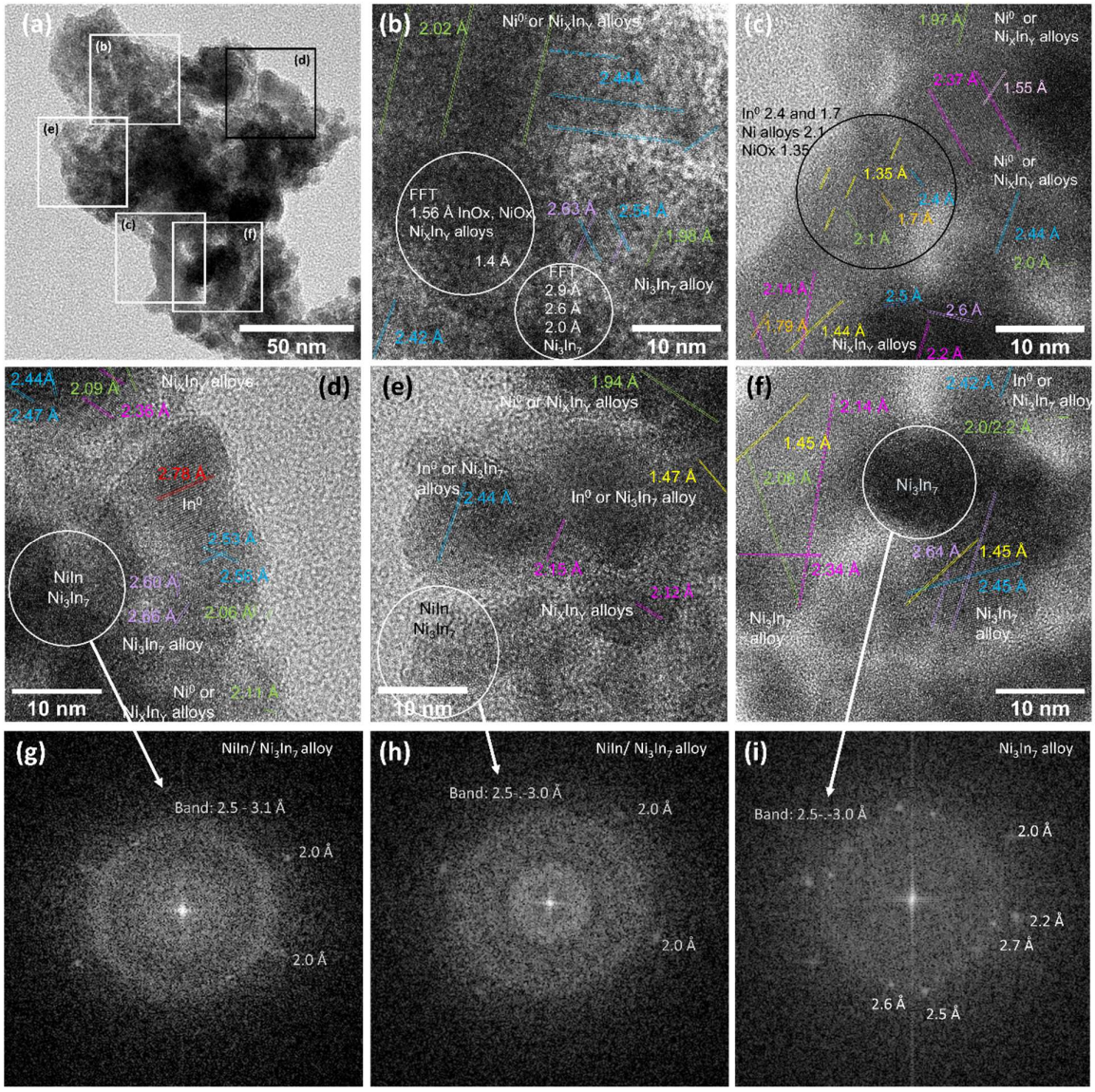


**Figure S5. HRTEM analysis of $Ni_{40}In_{60}Ox$ thin film after $CO_2$ER electrolysis in 0.1 M $KHCO_3$ at -0.8 V for 1h. (a) TEM micrograph of investigated region. (b-f) high resolution images of corresponding areas labeled in image (a). (g-i) FFT analysis of marked areas in images (d-f). HRTEM resolution is 0.0194 pix/nm.**

The analysis of HRTEM data indicates the formation of $Ni^0$ and/or $Ni_XIn_Y$ crystallites mainly NiIn and $Ni_3In_7$ and a few $In^0$. The highly amorphous material was analyzed by FFT and revealed the presence of very small domain with d spacings typical of $Ni_XIn_Y$ (NiIn and $Ni_3In_7$) and oxidic phases NiO and $In_2O_3$. The persistence of oxidized Ni and In was further confirmed by HAADF-STEM-EDS indicating the persistence of oxygen in the material even on a sample protected from oxidation in air prior EDS analysis (Figure S9c).

**Table S4. Details on d-spacing assignment on HRTEM micrographs images of $Ni_{40}In_{60}Ox$ after $CO_2ER$ electrolysis in 0.1 M $KHCO_3$ at -0.8 V for 1 h presented in Figure S5.**

| HRTEM of $Ni_{40}In_{60}Ox$ @ -0.8 V for 1 h | | | | | Possible phases | | | | | | |
|---|---|---|---|---|---|---|---|---|---|---|---|
| b | d | c | f | e | | | | | | | |
| | 2.76 | | | | $In^0$ (2.72) | | | | | | |
| 2.63 | 2.57 | | 2.61 | | $Ni_3In_7$ (2.65 Å) | | | | | | |
| 2.55<br>2.44 | | 2.51<br>2.44 | 2.44 | 2.45 | $In^0$ (2.48 Å) | $In_2O_3$ (2.53 Å) | NiO (2.55 Å) | $Ni_3In_7$ (2.46 Å) | | | |
| 2.38 | 2.37 | 2.37<br>2.29 | 2.33 | | $In^0$ (2.30 Å) | NiO (2.21 Å) | $Ni^0$ (2.27 Å) | NiIn (2.27 Å) | $Ni_2In_3$ (2.20 Å) | | |
| | | 2.13 | 2.15 | 2.13 | $Ni^0$ (2.16 Å) | NiIn (2.17 Å) | $Ni_3In$ (2.10 Å) | $Ni_2In_3$ (2.17 Å) | $Ni_3In_7$ (2.17 Å) | | |
| 1.99 | 2.09 | 1.97 | 2.09<br>1.94 | 1.95 | $Ni^0$ (2.04 Å) | $Ni^0$ (2.01 Å) | NiIn (2.01 Å) | $Ni_3In_7$ (2.05 Å) | | | |
| | | 1.8 | 1.83 | | $In_2O_3$ (1.79 Å) | $Ni^0$ (1.77 Å) | NiIn (1.79 Å) | | | | |
| 1.59 | | | | | $In^0$ (1.69 Å) | $Ni_3In_7$ (1.59 Å) | | | | | |
| 1.55 | | 1.55<br>1.43 | 1.45 | 1.47 | $In_2O_3$ (1.53 Å) | NiO (1.56 Å) | $Ni^0$ (1.57 Å) | NiIn (1.57 Å) | $Ni_3In$ (1.48 Å) | $Ni_2In_3$ (1.54 Å) | $Ni_3In_7$ (1.58 Å) |
| 1.4 | 1.34 | 1.34 | 1.35 | | $In^0$ (1.40) | NiO (1.33 Å) | | | | | |

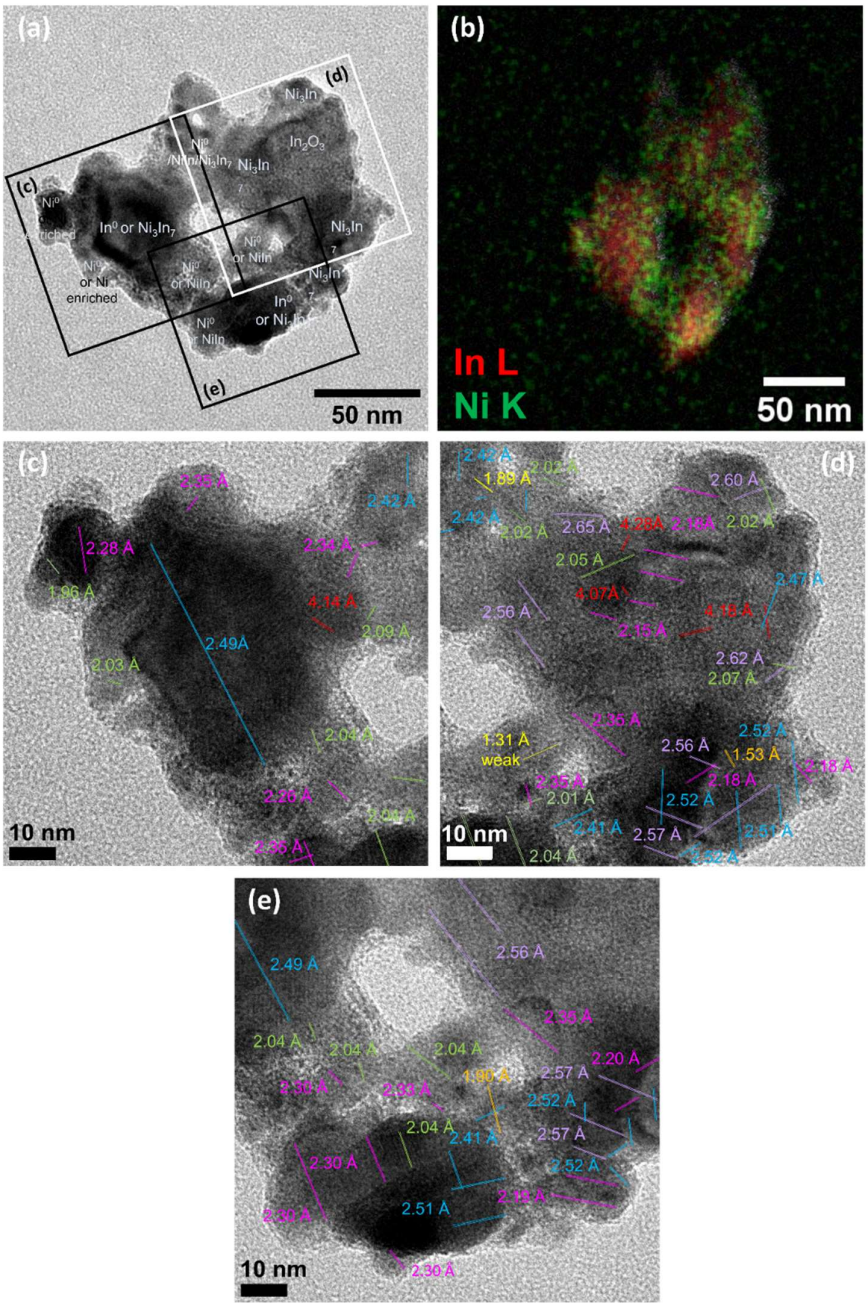


**Figure S6. HRTEM analysis of $Ni_{40}In_{60}O_X$ thin film after $CO_2$ER electrolysis in 0.1 M $KHCO_3$ at -1.0 V for 1h. (a) TEM micrograph of investigated region. (b) STEM-EDS Ni-In elemental mapping. (c-e) high resolution images of corresponding areas labeled in image (a). HRTEM resolution is 0.011 pix/nm.**

The analysis of HRTEM data in correlation with the HAADF-STEM-EDS mapping indicates the formation of an interconnected array of $In^0$ and $Ni_3In_7$ alloy grains, decorated with smaller Ni -rich grains composed by NiIn, $Ni^0$ and/or NiO. The HAADF-STEM-EDS was conducted on a sample a sample protected from oxidation in air prior analysis (Figure S9e). It reveals minimum O content, indicating complete reduction of original $Ni_{40}In_{60}Ox$ oxide.

**Table S5. Details on d-spacing assignment on HRTEM micrographs images of $Ni_{40}In_{60}Ox$ after $CO_2ER$ electrolysis in 0.1 M $KHCO_3$ at -1.0 V for 1h presented in Figure S6.**

| HRTEM of $Ni_{40}In_{60}Ox$ @ -1.0 V for 1 h | | | Possible phases | | | | | | |
|---|---|---|---|---|---|---|---|---|---|
| c | d | e | | | | | | | |
| 4.18 | 4.18 | | $In_2O_3$ (4.13 Å) | | | | | | |
| | 2.61 | | $Ni_3In_7$ (2.65 Å) | $In^0$ (2.72 Å) | | | | | |
| 2.49 | 2.54 | 2.51<br>2.41 | $In^0$ (2.48 Å) | $In_2O_3$ (2.53 Å) | NiO (2.55 Å) | $Ni_3In_7$ (2.46 Å) | | | |
| 2.29 | 2.26 | 2.35<br>2.29 | $In^0$ (2.30 Å) | NiO (2.21 Å) | $Ni^0$ (2.27 Å) | NiIn (2.27 Å) | $Ni_2In_3$ (2.20 Å) | | |
| | 2.14 | | $Ni^0$ (2.16 Å) | NiIn (2.17 Å) | $Ni_3In$ (2.10 Å) | $Ni_2In_3$ (2.17 Å) | $Ni_3In_7$ (2.17 Å) | | |
| 2.04 | 2.07 | 2.04 | $Ni^0$ (2.04 Å) | $Ni^0$ (2.01 Å) | NiIn (2.01 Å) | $Ni_3In_7$ (2.05 Å) | | | |
| | | 1.91 | $NiCO_3$ (1.93 Å) | | | | | | |
| | | | $In^0$ (1.69 Å) | $Ni_3In_7$ (1.59 Å) | | | | | |
| 1.54<br>1.47 | 1.54<br>1.47 | | $In_2O_3$ (1.53 Å) | NiO (1.56 Å) | $Ni^0$ (1.57 Å) | NiIn (1.57 Å) | $Ni_3In$ (1.48 Å) | $Ni_2In_3$ (1.54 Å) | $Ni_3In_7$ (1.58 Å) |
| | 1.4 | | $In^0$ (1.4 Å) | NiO (1.33 Å) | | | | | |
| 1.26 | 1.25 | | | NiO (1.28 Å) | $Ni^0$ (1.25 Å) | $Ni_3In$ (1.19 Å) | $Ni_2In_3$ (1.26 Å) | $Ni_3In_7$ (1.25 Å) | |

**Table S6. Details on d-spacing assignment on HRTEM micrographs images of $Ni_{40}In_{60}Ox$ after $CO_2ER$ electrolysis in 0.1 M $KHCO_3$ at -0.8 V for 10h presented in Figure S7**

| HRTEM of $Ni_{40}In_{60}Ox$ @ -0.8 V for 10 h | | | | | Possible phases | | | | | |
|---|---|---|---|---|---|---|---|---|---|---|
| b | c | d | e | f | | | | | | |
| | | | 2.91 | | $Ni_3In_7$ (2.91 Å) | | | | | |
| 2.67<br>2.64 | 2.69 | 2.71<br>2.68 | 2.63 | 2.63 | $Ni_3In_7$ (2.65 Å) | $In^0$ (2.72 Å) | | | | |
| 2.43 | 2.35<br>2.21 | 2.37 | 2.45 | | $In^0$ (2.48 Å) | $In_2O_3$ (2.53 Å) | NiO (2.55 Å) | $Ni_3In_7$ (2.46 Å) | | |
| | 2.16 | | | | $In^0$ (2.30 Å) | NiO (2.21 Å) | $Ni^0$ (2.27 Å) | NiIn (2.27 Å) | $Ni_2In_3$ (2.20 Å) | |
| | | | | | $Ni^0$ (2.16 Å) | NiIn (2.17 Å) | $Ni_3In$ (2.10 Å) | $Ni_2In_3$ (2.17 Å) | $Ni_3In_7$ (2.17 Å) | |
| | | | 2.05<br>1.98 | 2.04<br>2.05 | $Ni^0$ (2.04 Å) | $Ni^0$ (2.01 Å) | NiIn (2.01 Å) | $Ni_3In_7$ (2.05 Å) | | |
| 1.79 | 1.77 | 1.79 | | | $In_2O_3$ (1.79 Å) | $Ni^0$ (1.77 Å) | NiIn (1.79 Å) | | | |
| | | | 1.61 | 1.61 | $In^0$ (1.69 Å) | $Ni_3In_7$ (1.59 Å) | | | | |
| 1.34 | 1.31 | 1.31 | 1.33 | | $In^0$ (1.4 Å) | NiO (1.33 Å) | | | | |
| 1.20 | 1.15 | 1.20 | | | | NiO (1.28 Å) | $Ni^0$ (1.25 Å) | $Ni_3In$ (1.19 Å) | $Ni_2In_3$ (1.26 Å) | $Ni_3In_7$ (1.25 Å) |

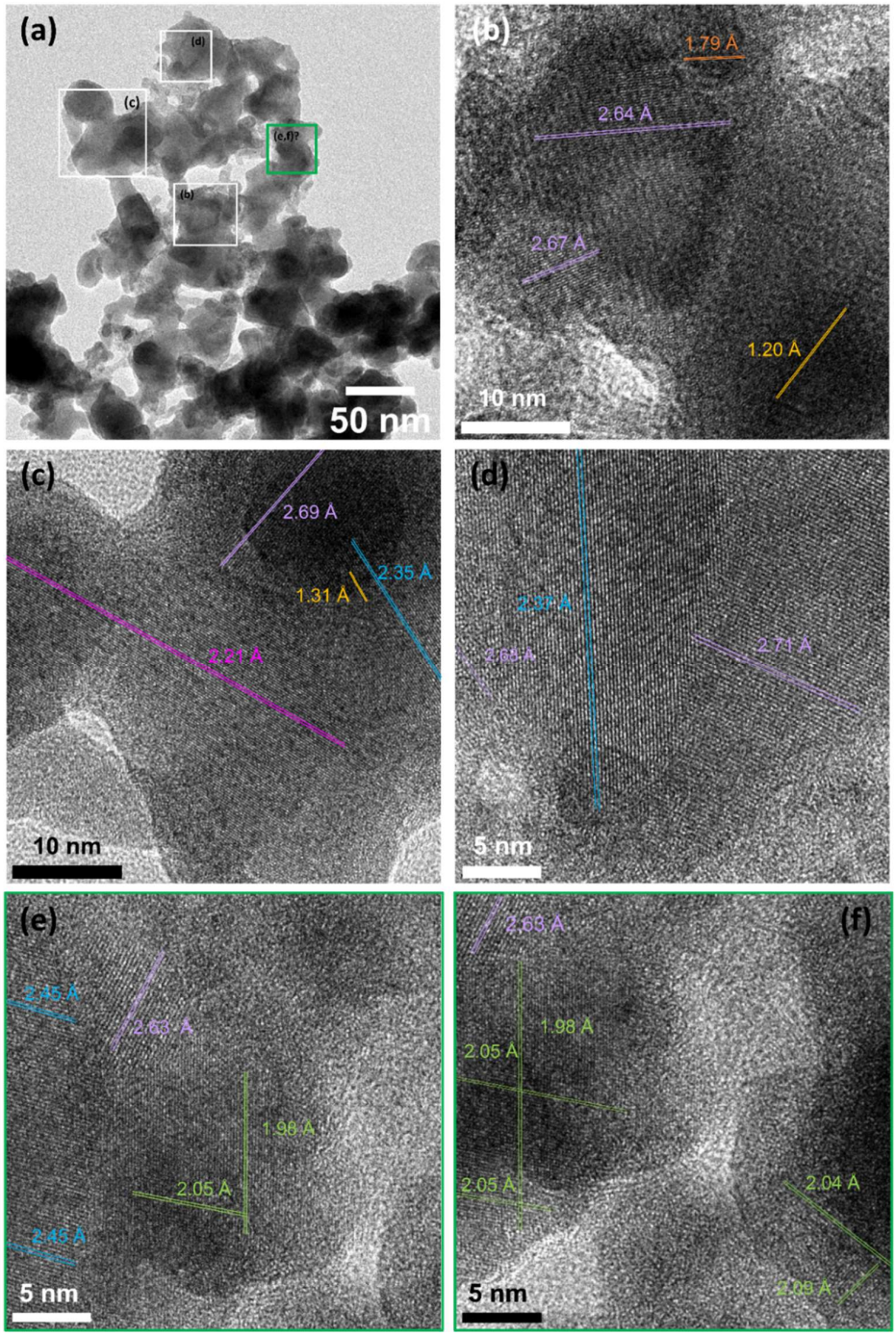


**Figure S7. HRTEM analysis of $Ni_{40}In_{60}O_X$ thin film after $CO_2$ER electrolysis in 0.1 M $KHCO_3$ at -0.8 V for 10h. (a) TEM micrograph of investigated region. (b-f) high resolution images of corresponding areas labeled in image (a). HRTEM resolution for images b-c is 0.019 pix/nm and 0.013 pix/nm for images d-f.**

The analysis of HRTEM data indicates the formation $Ni_XIn_Y$ alloys grains predominantly $Ni_3In_7$

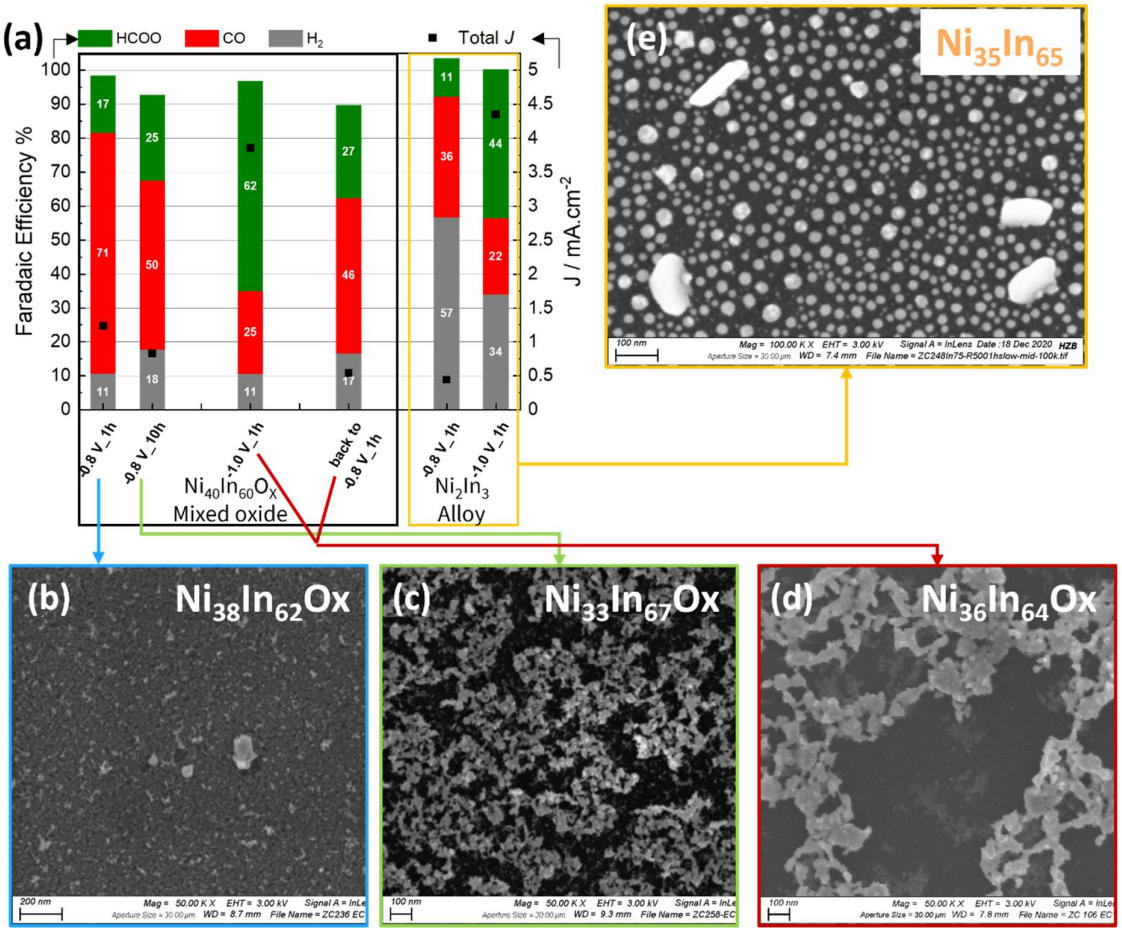


**Figure S8. Correlation of (a) $CO_2$ER activity of $Ni_{40}In_{60}Ox$ thin film and structural changes observed by SEM during in situ reduction at (b) -0.8 V for 1h; (c) -0.8V for 10h and (d) -1.0V for 1h, in comparison to (d) $Ni_2In_3$ alloys nanoparticles**

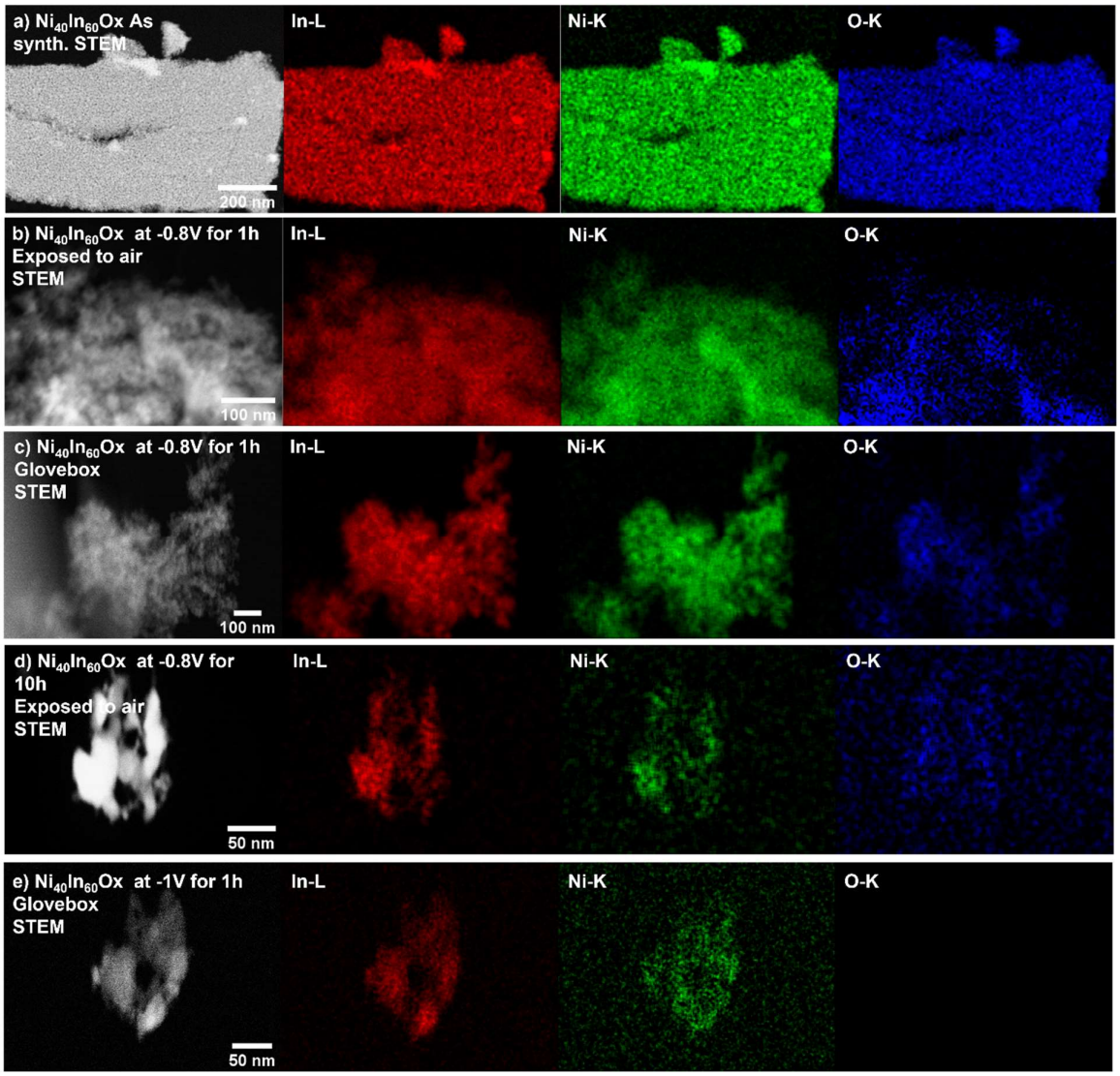


**Figure S9. Complimentary HAADF-STEM-EDS mapping of $Ni_{40}In_{60}Ox$ including oxygen distribution. From top to bottom. The EDS mappings for (a) As synthesized sample (exposed to air) and after $CO_2$ER at (b) -0.8 V for 1h ( exposed to air), (c) -0.8 V for 1h (handled in glovebox to prevent air exposure), (d) -0.8 V for 10h (exposed to air) and (e) -1.0 V for 1h (handled in glovebox to prevent air exposure ).**

The EDS mappings presented in Figure S9c,e were conducted on samples $Ni_{40}In_{60}Ox$ tested for $CO_2$ER inside an $O_2$-free glovebox and transferred to the TEM under inert atmosphere prior EDS analysis to prevent oxidation due to contact with air. In this manner the catalysts' structure can be investigated in a condition close to the *in situ* conditions. The so obtained results show that the sample tested at -0.8V for 1h (Figure S9c) display appreciable oxygen content indicating a persistence of oxide phases in this condition. In contrast the sample tested at -1.0V for 1h (Figure S9e) does not display detectable oxygen content, indicating a complete reduction of the original $Ni_{40}In_{60}Ox$ under this potential.

## Double layer capacitance measurements

The roughness was measured electrochemically performing cyclic voltammetry experiments between OCP ±100 mV at different sweeping rates between 10mVs$^{-1}$ and 500mVs$^{-1}$. Representative CV sets for $Ni_{40}In_{60}Ox$ derivatives are shown in the image below. The capacitive currents (anodic and cathodic) recorded at the OCP are plotted as a function of sweeping rate (***v***). The slope of the obtained linear plot corresponds to the double layer capacitance ($C_{DL}$) according to equation S1.

$$J = C_{DL} * v \qquad \text{Equation S1}$$

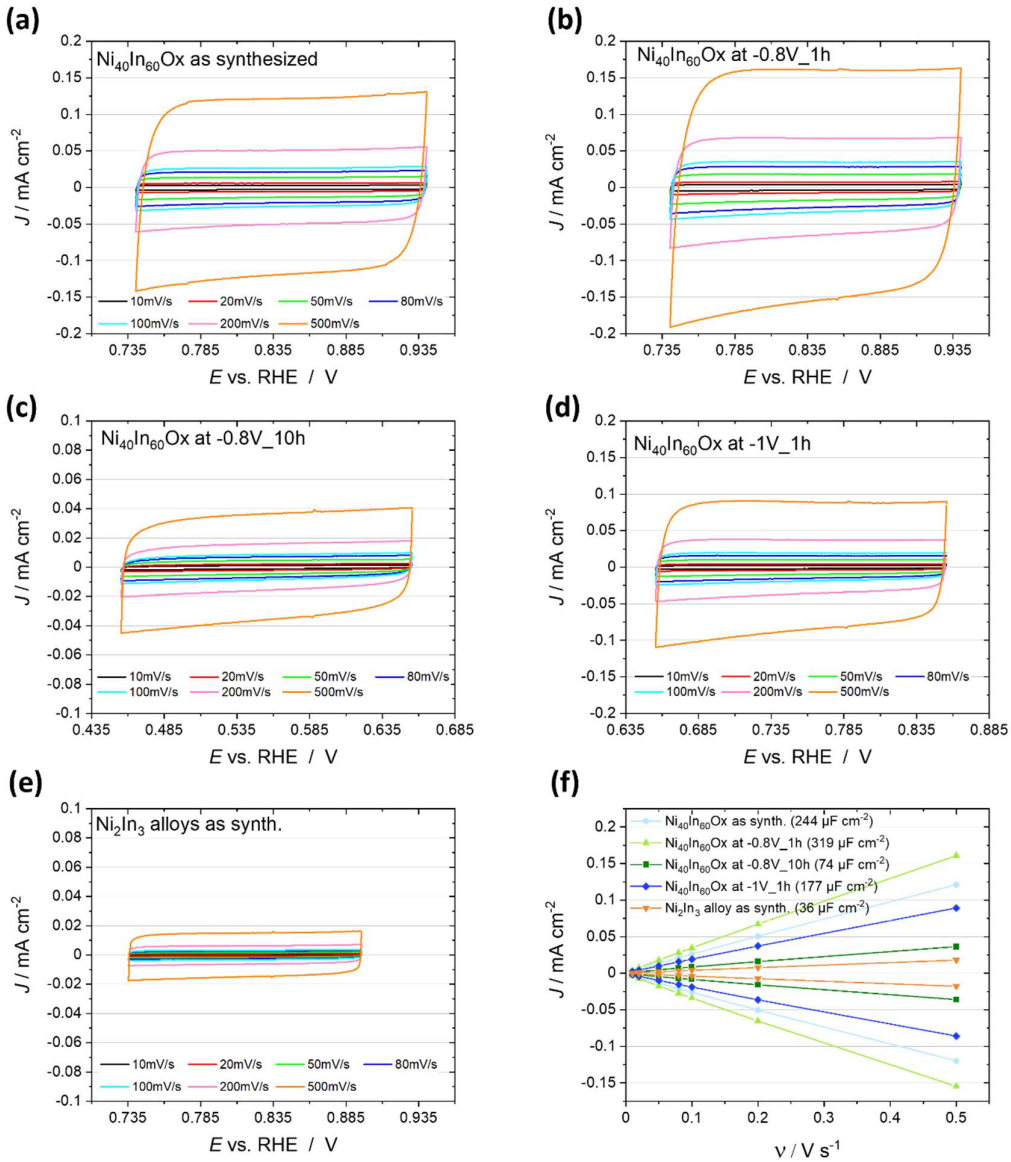


**Figure S10. Double layer capacitance $C_{DL}$ measurements by cyclic voltammetry in $N_2$ saturated 0.1 M $KHCO_3$ (pH 8.9) around OCP at sweeping rates from 5 mV s$^{-1}$ to 500 mV s$^{-1}$ for $Ni_{40}In_{60}Ox$ thin films (a) as synthesized and after electrolysis at (b) -0.8 V for 1 h, (c) -0.8 V for 10 h and (d) -1 V for 1h as well as (e) $Ni_2In_3$ alloy. (f) Plot of anodic and cathodic current density as a function sweeping rate for the different samples. ($E_{RHE} = E_{Ag/AgCl}$ + 0.211+ 0.0591×pH).**

## Gas chromatography method

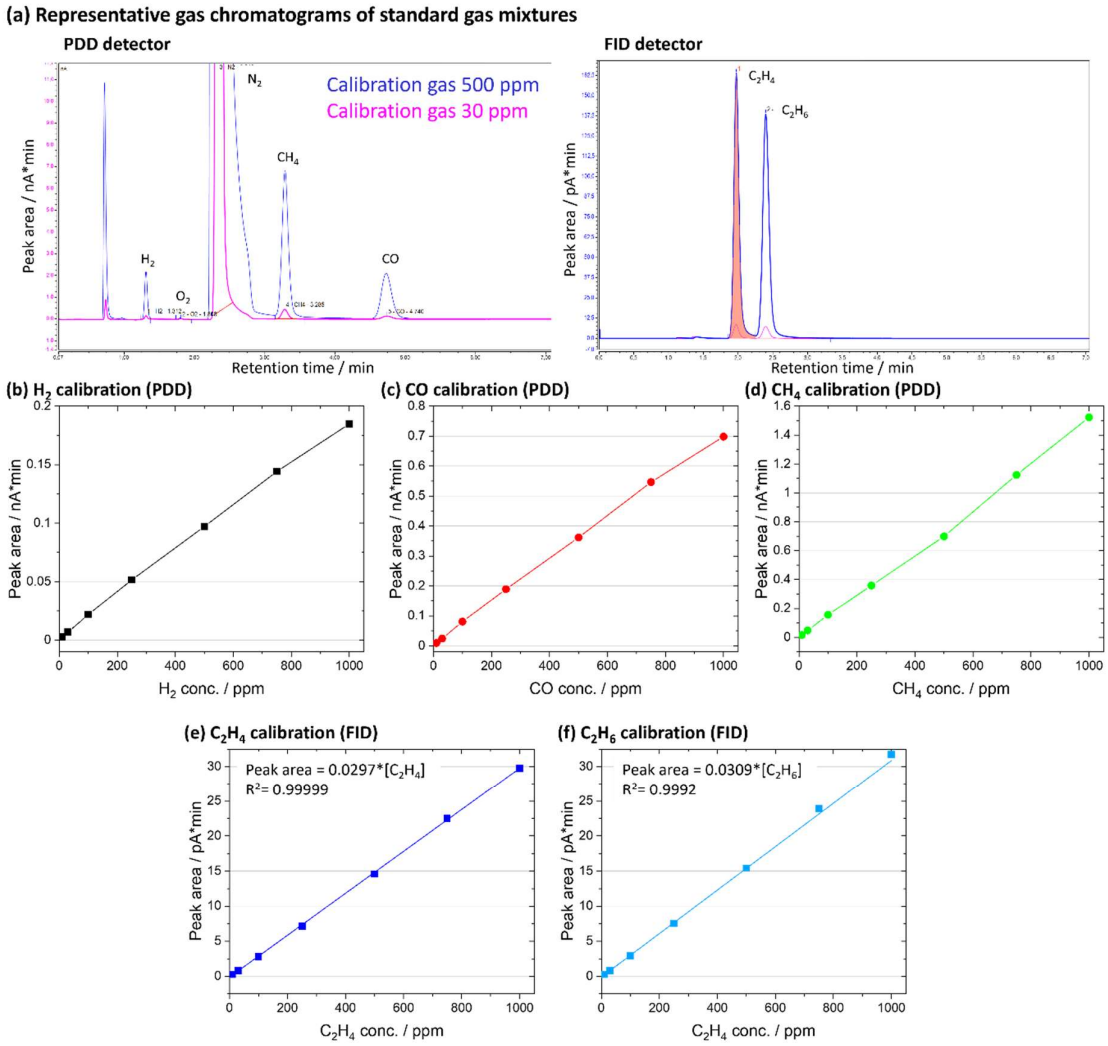


**Figure S11. Gas chromatography method details. (a) Representative chromatograms with PDD detector (left) and FID detector (Right) for standard gas mixtures of 30 ppm (pink) and 500 ppm (blue). Calibration curve for (b) $H_2$-PDD, (c) CO-PDD, (d) $CH_4$-PDD, (e) $C_2H_4$-FID and () $C_2H_6$-FID. Note that components detected on the FID are quantified using a linear regression. For components detected on the PDD detector a Point-Point calibration mode from Chromeleon software (Thermoscientific) is used.**

## HPLC method

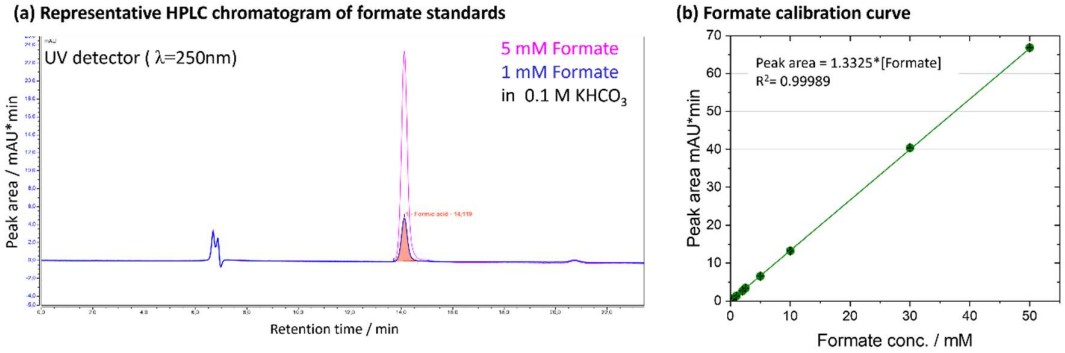


**Figure S12. HPLC method details. (a) Representative chromatograms for 5 mM (pink) and 1 mM(blue) formate standards in 0.1 M $KHCO_3$. (b) Calibration curve for formate.**

**Table S7. Comparison of $CO_2$ER activity of the catalysts in present study with previous literature reports.**

| Ref | Catalysts | Electrolyte | pH | *E* V RHE | *J* mAcm$^{-2}$ | $CO_2$ER selectivity | | | | Catalyst loading | | | |
|---|---|---|---|---|---|---|---|---|---|---|---|---|---|
| | | | | | | $FE_{CO}$ | $J_{CO}$ | $FE_{HCOO}$ | $J_{HCOO}$ | Mass µg cm$^{-1}$ | *Jmass*[a)] A/g | η µmol cm$^{-1}$ | *Jη*[a)] mA/µmol |
| this work | $Ni_{40}In_{60}Ox$ -0.7V | 0.1M $KHCO_3$ | 6.8 | -0.7 | 0.5 | 71 | 0.36 | 5.2 | 0.03 | 8.1 | 43.7 | 0.089 | 4.0 |
| | $Ni_{40}In_{60}Ox$ -0.8V | | 6.8 | -0.8 | 1.2 | 71 | 0.85 | 17 | 0.20 | 8.1 | 104.9 | 0.089 | 9.5 |
| | $Ni_{25}In_{75}Ox$ -0.7V | 0.1M $KHCO_3$ | 6.8 | -0.7 | 0.5 | 73 | 0.37 | 12 | 0.06 | 8.2 | 44.6 | 0.084 | 4.4 |
| | $Ni_{25}In_{75}Ox$ -0.8V | | 6.8 | -0.8 | 1 | 60 | 0.60 | 22 | 0.22 | 8.2 | 73.4 | 0.084 | 7.2 |
| | $Ni_{10}In_{90}Ox$ -0.7V | 0.1M $KHCO_3$ | 6.8 | -0.7 | 0.5 | 60 | 0.30 | 26 | 0.13 | 8.6 | 15.2 | 0.079 | 3.8 |
| | $Ni_{10}In_{90}Ox$ -1V | | 6.8 | -1 | 5.6 | 13 | 0.73 | 79 | 4.42 | 8.6 | 516.5 | 0.079 | 55.8 |
| | $In_2O_3$ -0.7V | 0.1M $KHCO_3$ | 6.8 | -0.7 | 0.3 | 18 | 0.05 | 79 | 0.24 | 12.6 | 4.3 | 0.109 | 0.5 |
| | $In_2O_3$ -1V | | 6.8 | -1 | 4 | 5.7 | 0.23 | 90 | 3.60 | 12.6 | 286.7 | 0.109 | 32.9 |
| 1 | $Ni_{0.02}In_{0.98}$ | 0.5M $NaHCO_3$ | 7.2 | -0.7 | 1.5 | 60 | 0.90 | | | 1819.2 | 0.5 | 16 | 0.056 |
| | $Ni_{0.25}In_{0.75}$ | | 7.2 | -0.7 | 2.2 | 25 | 0.55 | | | 1612.6 | 0.3 | 16 | 0.034 |
| 2 | Ni-$In_2O_3$ @C NFs GDE | 1M KOH | 14 | -0.8 | 185 | | | 93.6 | 173.16 | 1500.0 | 115.4 | 10.8 | 16.0 |
| | Ni-$In_2O_3$ @C NFs GDE | | 14 | -1 | 358 | | | 90 | 322.20 | 1500.0 | 214.8 | 10.8 | 29.8 |
| | $In_2O_3$ @C NFs GDE | 1M KOH | 14 | -0.8 | 140 | | | 85 | 119.00 | 1500.0 | 79.3 | 10.8 | 11.0 |
| | $In_2O_3$ @C NFs GDE | | 14 | -1 | 260 | | | 80 | 208.00 | 1500.0 | 138.7 | 10.8 | 19.2 |
| 3 | C-Cu/SnO2-0.8 core shell NP | 0.5M $NaHCO_3$ | 7.2 | -0.8 | 15 | 90 | 13.50 | | | 13469.4 | 1.0 | 188.994 | 0.1 |
| | C-Cu/SnO2-1.8 core shell NP | | 7.2 | -0.8 | no info | | | 85 | | 14285.7 | | 178.359 | |
| 4 | Cu20Sn Bronze NP ~100nm | 0.1M $KHCO_3$ | 6.8 | -0.9 | 2 | 90 | 1.80 | | | 1000.0 | 1.8 | 15.082 | 0.1 |
| | Cu6Sn5 Bronze NP ~100nm | | 6.8 | -1.17 | 6 | | | 73 | 4.38 | 1000.0 | 4.4 | 11.316 | 0.4 |
| 5 | FeNG-p (0.36wt.% Fe) Fe sites on N-graphene | 0.1M $KHCO_3$ | 6.8 | -0.67 | 5.8 | 80 | 4.64 | | | 10.8 | 429.6 | 0.193 | 24.0 |
| 6 | FeNC (2.14 wt% Fe) Fe on N doped carbon | 0.1M $KHCO_3$ | 6.8 | -0.65 | 6.9 | 42 | 2.90 | | | 64.2 | 45.2 | 1.150 | 2.5 |
| | NiNC (2.83 wt.% Ni) Ni on N doped carbon | | 6.8 | -0.75 | 8.5 | 96 | 8.20 | | | 84.9 | 96.6 | 1.447 | 5.7 |
| 7 | Ni-NG (0.44 wt.% Ni) Ni sites on N-graphene | 0.5M $KHCO_3$ | 7.2 | -0.62 | 11 | 95 | 9.20 | | | 4.4 | 2090.9 | 0.075 | 122.7 |

Note that red or green shading indicate the main product is CO or formate respectively. [a)]The corresponding ***Jmass*** and ***Jη*** presented are calculated for the main product.

## References


1 J. He, K. E. Dettelbach, D. A. Salvatore, T. Li and C. P. Berlinguette, *Angew. Chemie - Int. Ed.*, 2017, **56**, 6068–6072.

2 Z. Chen, G. Yu, B. Li, X. Zhang, M. Jiao, N. Wang, X. Zhang and L. Liu, *ACS Catal.*, 2021, **11**, 14596–14604.

3 Q. Li, J. Fu, W. Zhu, Z. Chen, B. Shen, L. Wu, Z. Xi, T. Wang, G. Lu, J. J. Zhu and S. Sun, *J. Am. Chem. Soc.*, 2017, **139**, 4290–4293.

4 A. Vasileff, C. Xu, L. Ge, Y. Zheng and S. Z. Qiao, *Chem. Commun.*, 2018, **54**, 13965–13968.

5 F. Pan, B. Li, E. Sarnello, Y. Fei, X. Feng, Y. Gang, X. Xiang, L. Fang, T. Li, Y. H. Hu, G. Wang and Y. Li, *ACS Catal.*, 2020, **10**, 10803–10811.

6 F. Pan, W. Deng, C. Justiniano and Y. Li, *Appl. Catal. B Environ.*, 2018, **226**, 463–472.

7 K. Jiang, S. Siahrostami, T. Zheng, Y. Hu, S. Hwang, E. Stavitski, Y. Peng, J. Dynes, M. Gangisetty, D. Su, K. Attenkofer and H. Wang, *Energy Environ. Sci.*, 2018, **11**, 893–903.